CB307: A Dual Targeting Costimulatory Humabody V_H Therapeutic for Treating PSMA-Positive Tumors

Sophie Archer[1], Phillip M. Brailey[1], Minjung Song[1], Phillip D. Bartlett[1], Ines Figueiredo[2], Bora Gurel[2], Christina Guo[2,3], Verena Brucklacher-Waldert[1], H. Lorraine Thompson[1], Jude Akinwale[1], Samantha E. Boyle[1], Christine Rossant[1], Neil R. Birkett[1], Julia Pizzey[1], Mark Maginn[1], James Legg[1], Richard Williams[1], Colette M. Johnston[1], Philip Bland-Ward[1], Johann S. de Bono[2,3], and Andrew J. Pierce[1]

ABSTRACT

Purpose: CD137 is a T- and NK-cell costimulatory receptor involved in consolidating immunologic responses. The potent CD137 agonist urelumab has shown clinical promise as a cancer immunotherapeutic but development has been hampered by on-target off-tumor toxicities. A CD137 agonist targeted to the prostate-specific membrane antigen (PSMA), frequently and highly expressed on castration-resistant metastatic prostate cancer (mCRPC) tumor cells, could bring effective immunotherapy to this immunologically challenging to address disease.

Experimental Design: We designed and manufactured CB307, a novel half-life extended bispecific costimulatory Humabody V_H therapeutic to elicit CD137 agonism exclusively in a PSMA-high tumor microenvironment (TME). The functional activity of CB307 was assessed in cell-based assays and in syngeneic mouse antitumor pharmacology studies. Nonclinical toxicology and toxicokinetic properties of CB307 were assessed in a good laboratory practice (GLP) compliant study in cynomolgus macaques.

Results: CB307 provides effective CD137 agonism in a PSMA-dependent manner, with antitumor activity both *in vitro* and *in vivo*, and additional activity when combined with checkpoint inhibitors. A validated novel PSMA/CD137 IHC assay demonstrated a higher prevalence of CD137-positive cells in the PSMA-expressing human mCRPC TME with respect to primary lesions. CB307 did not show substantial toxicity in nonhuman primates and exhibited a plasma half-life supporting weekly clinical administration.

Conclusions: CB307 is a first-in-class immunotherapeutic that triggers potent PSMA-dependent T-cell activation, thereby alleviating toxicologic concerns against unrestricted CD137 agonism.

Introduction

Prostate cancer is the most common lethal male malignancy, with high morbidity associated with metastatic disease. Unlike other tumor histologies where immunotherapy has been transformative for patient outcomes, results in prostate cancer have been disappointing (1).

Prostate-specific membrane antigen (PSMA; HGNC:FOLH1) is frequently and highly expressed by prostate cancer. PSMA is involved in glutamate and folate mobilization, uptake, and signaling, with wide-ranging oncogenic functions, including activation of the PI3K–AKT–mTOR pathway, cellular bioenergetics, and the DNA damage repair response (2). PSMA has also been reported on the neovasculature of nonprostate solid tumors (3–5), but not on normal vasculature (6).

PSMA is an attractive tumor antigen for both prostate cancer disease imaging and therapeutics due to its high prevalence in prostatic tissue (7) including a trend towards greater expression during the course of disease progression (2). PSMA-specific PET imaging agents have been shown to be more accurate at imaging prostate cancer than traditional CT and bone scan techniques (8) and have been widely adopted in clinical practice (9). High clinical response rates to ^{177}Lu-PSMA radioligand (10) and the subsequent regulatory approval of ^{177}Lu vipivotide tetraxetan provide further support for therapeutic targeting of PSMA in prostate cancer.

CD137 (HGNC:TNFRSF9, also known as 4–1BB), is a member of the TNFR superfamily primarily expressed on the surface of activated T cells as a costimulatory receptor. In combination with other signals, CD137 agonism enhances T-cell cytotoxicity and proliferation (11, 12) and drives T-cell mitochondrial function and metabolism (13, 14), increases cytokine production (15), and promotes T-cell survival through upregulation of survival genes *BCL-xL* and *BFL-1* (16). CD137 function is activated by molecular clustering of CD137 monomers driven ordinarily by interaction with the homotrimeric CD137 cognate ligand TNFSF9 (17, 18), a mechanism shared by other TNFR superfamily members (19).

Despite these attractive functional properties and early signs of clinical activity with CD137 agonist mAbs, the therapeutic window has been limited by on-target off-tumor treatment-related liver toxicity (20). Attempts to circumvent such toxicity with either reduced exposure to more potent CD137 agonist antibodies, or administration of reduced potency CD137 agonist antibodies (21), have thus far met with limited success.

To address the unmet medical need for effective immunotherapy in metastatic castration-resistant prostate cancer while avoiding systemic toxicity, we developed the novel immunotherapeutic CB307. Mechanistically, CB307 is designed to bridge PSMA-expressing tumor cells and CD137-expressing T cells to induce PSMA-dependent CD137 clustering on T cells. CB307 is a Humabody single-polypeptide chain made of three peptide-linked fully human heavy chain variable (V_H)

[1]Crescendo Biologics Ltd., Babraham Research Campus, Cambridge, United Kingdom. [2]Cancer Biomarkers Group, The Institute of Cancer Research, London, United Kingdom. [3]Prostate Cancer Targeted Therapies Group, Royal Marsden Hospital, Sutton, United Kingdom.

Corresponding Authors: Andrew J. Pierce, Translational Biology, Crescendo Biologics, Meditrina Building 260, Cambridge, Cambridgeshire, CB22 3AT, UK. E-mail: apierce@crescendobiologics.com; and Sophie Archer, Crescendo Biologics Ltd., Meditrina Building 260, Babraham Research Campus, Cambridge, CB22 3AT, UK. E-mail: sarcher@crescendobiologics.com

Clin Cancer Res 2024;30:1595–606

doi: 10.1158/1078-0432.CCR-23-3052

Translational Relevance

The first-in-class PSMA-directed CD137 agonist CB307 is in clinical development both as monotherapy and in combination with the anti-PD-1 checkpoint inhibitor pembrolizumab to treat cancers including metastatic castration-resistant prostate cancer (mCRPC). Herein, we present preclinical mechanistic evidence demonstrating antitumor immune responses induced by this novel approach. PSMA clusters CB307 to agonize CD137 on T cells but is not necessarily the target of the T cells themselves. Thereby, following tumor-antigen triggered activation of T cells by CB307, T cells continue to surveille polyclonal targets for tumor cell killing even should PSMA expression be heterogeneous or lost. Single-agent checkpoint inhibitor approaches in prostate cancer have been largely ineffective, highlighting the need for novel immunomodalities and combination-based approaches. Quantitative determination of CB307–pembrolizumab combination pharmacology indicates at least additive activity and supports this combinatorial clinical development strategy.

domains derived from the Crescendo transgenic mouse (22), where the individual V_H domains in CB307 monovalently target PSMA, CD137, and human serum albumin (HSA). The smaller molecular weight of CB307 (46 kDa) with respect to traditional mAbs may aid tumor penetration (23) while binding to HSA extends serum half-life (24) and may further improve biodistribution.

Here we describe for the first time the nonclinical pharmacology, toxicokinetics, and toxicology of CB307. We hypothesize that by restricting CD137 agonism to areas of PSMA expression, CB307 will induce potent, targeted T-cell activation in patients with $PSMA^+$ tumors while maintaining acceptable systemic tolerability, thereby overcoming therapeutic limitations of earlier generation CD137 agonists.

Materials and Methods

Generation of CB307

V_H generation methods and the Crescendo mouse platform are described in Teng and colleagues (22). CB307 consists of three peptide-linked V_H that bind the human targets PSMA, CD137, and HSA, respectively. Additional details are in Supplementary Materials and Methods.

CB307 kinetics

Kinetics of CB307 binding to PSMA, CD137, and HSA were assessed using a Biacore 8K (Cytiva) platform; 2 μg/mL F_c-tagged CD137 protein or 5 or 10 μg/mL F_c-tagged PSMA protein (Acro Biosystems) were captured on Protein G biosensors, 2.5 μg/mL HSA (Sigma) was immobilized directly on a CM5 biosensor, and CB307 binding was assessed in a 5-point 3-fold dilution series over a range of concentrations. After background subtraction, interactions were modeled on the basis of the expected 1:1 binding stoichiometry.

Cell lines and primary human cells

CHO cells (female; RRID:CVCL_4099) were purchased from Life Technologies; DU145 parental cells (male; RRID:CVCL_0105) were purchased from ATCC; LNCaP cells (male; RRID:CVCL_0395) were purchased from ECACC. Cell lines were not otherwise authenticated. Cultured cells are tested twice yearly for mycoplasma with a LookOut Mycoplasma PCR Detection Kit (Sigma). Cells were cultured for up to 20 passages and used in experiments between passage 5 and 20.

PSMA stably expressing cell line DU145-PSMA was generated in house by lentivirus transduction. Tetracycline-inducible CHO-CD137 and CHO-PSMA cells were made in house by plasmid transfection using lipofectamine. Prior to an experiment requiring induced expression, CD137 or PSMA expression was induced by addition of 1 μg/mL tetracycline for a minimum of 16 hours. DU145 parental, DU145-PSMA, and LNCaP cells were maintained in RPMI 1640 medium supplemented with 10% FBS, 2 mmol/L *L*-glutamine, 50 U/mL penicillin, and 50 μg/mL streptomycin. CHO cells were maintained in DMEM medium supplemented with 10% FBS, 2 mmol/L *L*-glutamine, 50 U/mL penicillin, and 50 μg/mL streptomycin. An isogenic PD-L1 gene knockout version of the DU145-PSMA cell line was commissioned using CRISPR technology (Synthego).

Peripheral blood mononuclear cells (PBMC) were isolated from leukocyte reduction system cones from healthy human donors by density gradient centrifugation over Lymphoprep (STEMCELL Technologies).

Dual binding assay

The capacity of CB307 to bind either PSMA-expressing or CD137-expressing cell lines and to simultaneously engage the second target (CD137 or PSMA, respectively) was measured using Fluorescence Microvolume Assay Technology (FMAT). Full details are found in Supplementary Materials and Methods.

Jurkat–NFκB–CD137 reporter assay

DU145-PSMA or DU145 parental cells were plated overnight in cell assay media (RPMI-based as above) with PBMCs in 384-well tissue culture plates. Serial dilutions of CB307 were prepared in cell assay media and added to plates followed by Jurkat human CD137 NFκB luciferase reporter gene cells (Promega). Where indicated, serial dilutions of vipivotide tetraxetan (Cambridge Bioscience) were added. After a 5.5-hour incubation at 37°C/5% CO_2, the level of luciferase reporter expression was determined by addition of Bio-Glo reagent (Promega) and measurement of luminescent signal on a PHERAstar FS plate reader (BMG Labtech).

In vitro 2D coculture assay

DU145-PSMA and DU145-Parent cells were plated in cell assay media in tissue culture plates with either anti-CD3 antibody or SEB (staphylococcal enterotoxin B) stimulation using serial dilutions of CB307 with various additional drug combinations. Full details are found in Supplementary Materials and Methods.

Drug synergy experiments were performed with CB307 and an anti-PD-1 antibody utilizing the *in vitro* 2D coculture assay methods with SEB stimulation described above. Drug synergy was assessed with the SynergyFinder online resource (25) using the Bliss/Loewe consensus scoring method.

In vitro NK coculture assay

NK cells were isolated from healthy human PBMCs using a Negative Selection Kit (STEMCELL) according to the manufacturer's instructions and activated with IL2 (BioLegend) for 24 hours. Activated NK cells were harvested and cocultured with DU145-PSMA or DU145-Parent cells at a plating ratio of 2 (NK) to 1 (DU145). Next, 1 nmol/L CB307 was prepared in assay media and added to the plates, which were subsequently incubated for 2 days at 37°C/5% CO_2. Supernatant was harvested and CCL3, CCL4, and IFNγ were quantified using human DuoSet reagents (R&D Systems).

In vitro 3D tumor spheroid cell killing assay

DU145-PSMA cells were transduced (MOI of 3) with mKate2 (RFP) encoding lentivirus (Sartorius) in the presence of 8 μg/mL polybrene. Transduced cells were selected for permanent expression of RFP using 2 μg/mL puromycin. RFP-DU145-PSMA cells were plated at 2.5×10^4 per well in a 96-well ultra-low adhesion plate for 24 hours prior to the addition of 1×10^5 PBMCs. The cells were treated with 25 nmol/L CB307, 25 nmol/L pembrolizumab, 25 nmol/L atezolizumab as monotherapy or in combination and 5 μg/mL anti-CD3 antibody (Clone OKT3; BioLegend). Plates were incubated inside an IncuCyte ZOOM Live-Cell analysis system (Essen Bioscience), during which live images were acquired every 2 hours. At the conclusion of the experiment after 10 days of coculture, cells were gently mechanically disaggregated by trituration and quantified for tumor and T-cell content by flow cytometry.

Flow cytometry

PSMA, PD-L1, and markers of immune activation were assessed using a Cytek Aurora flow cytometer; data were analyzed using FlowJo software (Becton, Dickinson & Company; RRID:SCR_008520). Full details are in Supplementary Materials and Methods.

Cytokine analysis

For PBMC and NK-cell coculture assays, soluble analytes in supernatants were analyzed using human DuoSet reagents (R&D Systems) according to the manufacturer's instructions with the following exceptions: capture antibody was coated on Multi-Array SECTOR plates (Meso Scale Discovery); biotinylated detection antibody was detected by 1 nmol/L streptavidin-SULFO-TAG reagent (Meso Scale Discovery); plates were read on an MSD Sector Imager and analyzed using MSD Workbench software.

CD137 and PSMA IHC

We developed a novel protocol for visualizing CD137 using chromogenic IHC. Briefly, a rabbit monoclonal anti-CD137 antibody (clone E6Z7F, #19541; Cell Signaling Technology) was diluted 1:100 in Bond primary antibody diluent (AR9352; Leica Biosystems), applied to formalin-fixed paraffin-embedded (FFPE) tissue following Bond Epitope Retrieval Solution 1 (ER1; AR9961; Leica Biosystems) antigen retrieval for 30 minutes and detected using the Bond Polymer Refine Detection Kit (DS9800; Leica Biosystems).

The assay was optimized and validated (Supplementary Fig. S1) by performing Western blotting of protein lysates and IHC staining of cell pellets from HDLM-2 cells (male; RRID:CVCL_0009) known to express cell-surface CD137 (26) treated with nonsilencing control siRNA compared with HDLM-2 cells treated with CD137-targeting siRNA (Supplementary Fig. S1A), as well as wild-type Jurkat cells (male; RRID:CVCL_0065), which express minimal CD137 (26) compared with CD137-transfected Jurkat cells treated with nonsilencing control siRNA and CD137-transfected Jurkat cells treated with CD137 targeting siRNA (Dharmacon; Supplementary Fig. S1B). Western blotting showed expected bands between 35 and 40 kDa and a decrease in both bands with knockdown and in the wild-type Jurkat cells compared with $CD137^+$ Jurkat cells (Supplementary Fig. S2). These findings were corroborated by IHC of contemporaneously collected cell pellets. Appropriate tissue localization for CD137 was observed by the pathologist (B.G.) in human tonsil, appendix, and normal prostate tissue (Supplementary Fig. S1C).

The CD137 IHC assay was subsequently developed in a dual-chromogenic PSMA/CD137 protocol, incorporating a previously validated PSMA IHC method. Full details are in Supplementary Materials and Methods.

We applied the dual-chromogenic PSMA/CD137 protocol to human castration-resistant prostate cancer (CRPC) biopsies from patients treated at the Royal Marsden Hospital. Tissue was collected from primary prostate tumors ($n = 10$) and metastatic prostate lesions from different anatomical contexts: bone marrow ($n = 19$), lymph node ($n = 20$), soft tissue ($n = 10$), and liver ($n = 10$). Using a pathologist-supervised HALO image analysis software (Indica Labs), we segmented tumor from stroma, and determined the percentage of PSMA-positive tumor cells as well as the density of CD137-expressing cells in each compartment.

Separately, three multitumor tissue microarrays (TMA: TissueArray LLC #BCN911, #MC1501A, #MC2082D) were stained (HistologiX) using the PSMA/CD137 dual-chromogenic protocol and images analyzed (OracleBio) to determine the percent of viable cells per core that were $PSMA^+$ and the number of $CD137^+$ cells per mm^2 of viable tissue on each core. Where duplicate cores were provided, results were averaged. Analysis was restricted to only those tumor types represented with at least 10 nonduplicate scorable cores.

CB307 pharmacokinetics in mice

CB307 is not cross-reactive with mouse serum albumin (MSA) so the feasibility of coadministration of HSA/drug was established as a method of half-life extension in mice in a dedicated mouse pharmacokinetic (PK) study conducted at TransCure bioServices, utilizing a highly related CB307 precursor molecule that like CB307 is a three V_H domain polypeptide with PSMA, CD137, and HSA binding specificities. Mice received a single dose of 3 mg/kg drug premixed with 10 mg/kg HSA or, alternatively, 3 mg/kg drug without exogenous HSA. Mice were either transgenic double-humanized for both serum albumin and the neonatal Fc receptor (FcRn) (groups 1 and 2: GenOway S.A.) or were NCG mice wild-type for both mouse serum albumin and mouse FcRn (groups 3 and 4: Charles River Laboratories). Mice transgenic for HSA and hFcRn display PK properties for HSA-binding drugs reflective of those expected in the human system (27) and serve as a positive control for the coadministered drug with exogenous HSA method of PK extension. Because of veterinary restrictions on the number of permissible blood draws per individual animal, groups were subdivided into subgroups of animals with interleaved blood sampling timepoints to collectively make up one complete PK profile. The study scheme is shown in Supplementary Fig. S3A. Detailed mouse PK methods are in Supplementary Materials and Methods.

Syngeneic mouse *in vivo* pharmacology antitumor activity study

Antitumor activity of CB307 was evaluated with an RM1 mouse (male; RRID:CVCL_B459) prostate cancer cell line engineered to express doxycycline-inducible human PSMA (Crown Bioscience: HuCell PSMA-RM1) implanted into C57BL/6 mice that are transgenic for exons 4 to 7 of human CD137 (Crown Bioscience: HuGEMM HUCD137). Each mouse was inoculated subcutaneously in the right rear flank region with 1×10^6 RM1-hPSMA tumor cells in 0.1 mL of PBS for tumor development. When mean tumor volume reached 69 mm^3, mice were randomly assigned to four groups with 10 mice per group in each of three CB307 dose/response arms and 12 mice in an HSA control group from which four were used to monitor the hPSMA expression level postinduction with doxycycline. Dosing of CB307/HSA was initiated 1 day after randomization. Mice were treated intraperitoneally with either HSA only at 10 mg/kg or with

CB307 co-dosed with HSA at 1 mg/kg + 10 mg/kg, 3 mg/kg + 10 mg/kg, and 10 mg/kg + 20 mg/kg, respectively. Mice were dosed both in the morning and again in the evening for daily doses nominally 8 and 16 hours apart. All groups received drinking water supplemented with doxycycline for continuous hPSMA induction after the start of treatment. Tumor volumes were measured with calipers twice per week after randomization.

Select tumors were quantified for hPSMA expression. Tumors were disaggregated into single-cell suspensions with a Miltenyi Tumor Dissociation Kit (#130–096–730) and the gentleMACS Octo dissociator (Miltenyi, #130–096–427). The resulting cell suspensions were filtered and enumerated. For each sample, 1×10^6 cells were treated with mouse Fc Block solution (#553141, BD Biosciences) for 10 minutes in the dark. Cells were stained with anti-mCD45-PerCP/CY5.5 (30-F11, #103132, BioLegend), anti-hPSMA-PE (LiN-17, #342503, BioLegend), and live/dead stain (eBiosciences, #65–0865–14) for 30 minutes at 4°C. Following the incubation, all samples were washed and subsequently analyzed on an LSRFortessa X-20 (BD Biosciences).

GLP toxicology study in nonhuman primates

An IND-enabling GLP-toxicology study evaluated the potential toxicity of CB307 when given by intravenous infusion for three doses (days 1, 8, and 15) over 3 weeks to cynomolgus macaques. Recovery animals were also included to determine the potential reversibility of any toxicologic findings. In addition, the TK characteristics of CB307 were determined.

The dosing strategy is given in Supplementary Fig. S3B. Three weekly doses were administered to male and female juvenile Mauritian cynomolgus macaques. Animals were between 23 and 27 months old and weighed between 2.3 and 3.5 kg at the initiation of dosing. In addition to a nondrug-dosed control group, CB307 groups were dosed at 1, 5, or 30 mg/kg. Detailed nonhuman primate (NHP) PK assessment methods are found in Supplementary Materials and Methods.

Ethical approvals

All studies involving human subjects were conducted in accordance with the Declaration of Helsinki, and consistent with the Belmont Report. Written informed consent was obtained from each subject.

NHP ethical approval

The in-life experimental procedures undertaken during the course of this study were subject to the provisions of the United Kingdom Animals (Scientific Procedures) Act 1986 Amendment Regulations 2012. The number of animals used was the minimum consistent with scientific integrity and regulatory acceptability, consideration having been given to the welfare of individual animals in terms of the number and extent of procedures to be carried out on each animal.

Mouse ethical approval

All mouse-based protocols and procedures were reviewed and approved by the Institutional Animal Care and Use Committee (IACUC) of CrownBio. The care and use of animals was conducted in accordance with the regulations of the Association for Assessment and Accreditation of Laboratory Animal Care (AAALAC).

Human primary tissue ethical approval and informed consent

Use of human primary tissue was approved under the Royal Marsden Hospital ethics committee protocol CCR2472, REC reference: 04/Q0801/60.

Primary human cells ethical approval

All healthy donor human blood cells were obtained with patient consent from the NHS Blood and Transfusion service at Addenbrooke's hospital, under East Midlands–Leicester South Research Ethics Committee approval, REC reference 20/EM/0100.

Availability of data and material

Data generated or analyzed are included in this published article and its Supplementary Information files. Raw data are available from the corresponding author(s) upon request.

Results

CB307 target binding-kinetics

A schematic of CB307 shows the individual V_H domains and separating peptide linkers that make up the molecule (**Fig. 1A**). CB307 bound to PSMA, CD137, and HSA with K_D of 6.2×10^{-11} M, 6.0×10^{-10} M, and 8.2×10^{-9} M, respectively. A full summary of binding kinetics (Supplementary Fig. S4A) and kinetic profiles of CB307 interacting with human PSMA, CD137, and HSA (Supplementary Fig. S4B) are given in Supplementary Data.

CB307 binding to cell-expressed targets

CB307 binding to target-expressing cell lines was measured using an FMAT dual-binding assay, demonstrating that CB307 can simultaneously bind cell-presented PSMA and soluble CD137 (Supplementary Fig. S5A), and likewise cell-presented CD137 and soluble PSMA (Supplementary Fig. S5B).

Detection of CB307 binding to cell-expressed PSMA was measured using Fc-tagged recombinant human CD137 protein and anti-Fc-AF488 antibody. CB307 bound to DU145-PSMA cells, engineered to express PSMA receptors, in a concentration-dependent manner, but not to DU145-Parent cells. The mean (±SD) EC_{50} for engagement to DU145-PSMA cells was 0.35 (±0.06) nmol/L ($n = 4$). Similarly, CB307 bound to LNCaP cells, which express native levels of PSMA, where the mean (±SD) binding EC_{50} was 0.22 (±0.06) nmol/L ($n = 4$).

CB307 binding to human or NHP PSMA was compared using CHO cells engineered to overexpress PSMA from either species. Here, CB307 bound with mean (±SD) EC_{50} of 0.25 (±0.04) nmol/L and 0.56 (±0.11) nmol/L for CHO-huPSMA and CHO-cyPSMA, respectively ($n = 4$).

CB307 binding to CD137-expressing cells was measured using biotinylated recombinant human PSMA protein and streptavidin-AF488. CB307 bound to CHO cells engineered to express human CD137 with a mean (±SD) EC_{50} of 0.20 (±0.05) nmol/L ($n = 4$). No binding of CB307 was detected on CHO-Parent cells.

CB307 requires PSMA-expressing cells for CD137 agonist activity

PSMA expression was analyzed in engineered prostate cell lines (**Fig. 1B**), confirming high expression in lines engineered to express PSMA, with PSMA levels equivalent to those in the natively PSMA-expressing, but less technically facile, tumor LNCaP cell line.

To assess the CB307 dependence upon PSMA expression in the local microenvironment, we used a CD137 reporter cell line (**Fig. 1C**) to measure CD137 signaling mediated by CB307 in an isogenic pair of PSMA-expressing (DU145-PSMA) and PSMA-nonexpressing cells (DU145-Parent). CB307 induced concentration-dependent increases in CD137 reporter gene expression when Jurkat–NFκB–CD137 reporter cells were cocultured with DU145-PSMA cells but not in cocultures containing DU145-Parent cells (**Fig. 1D**). The mean (±SD)

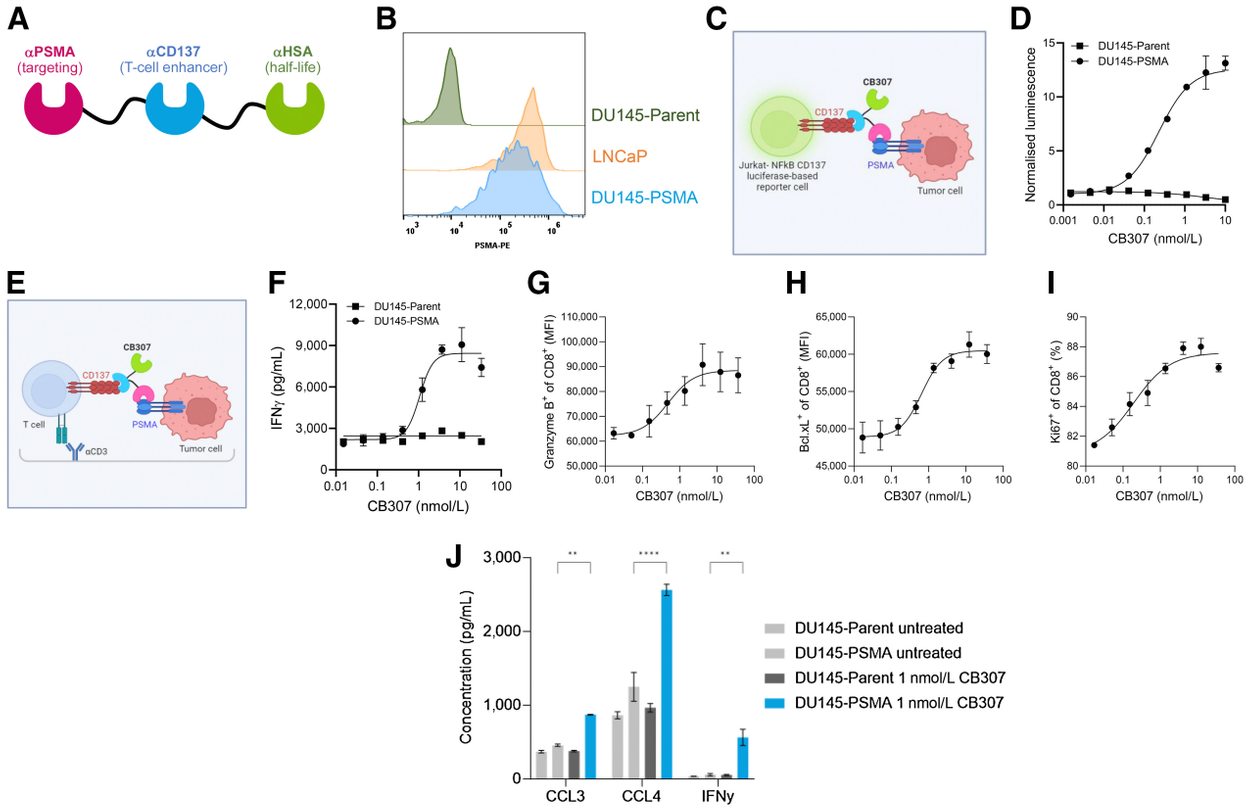

Figure 1.

CB307 design and induced T-cell phenotypes. **A,** Illustration of CB307 format: three V_H domains separated by peptide linkers. **B,** PSMA expression on cell lines. DU145-PSMA is isogenic to DU145-Parent other than for constitutive stable PSMA expression. **C,** Schematic of a Jurkat-based CD137 agonism reporter system whereby CB307 confers the clustering status of PSMA upon CD137 to generate a CD137 agonist signal. CD137 signaling is measured by luciferase expression from an NFκB-based reporter gene. **D,** Comparison of the reporter gene signal in the presence (DU145-PSMA) and absence (DU145-parent) of PSMA expression. **E,** Schematic of a primary cell CD137 activity assay whereby PBMCs stimulated by plate-bound αCD3 are co-incubated with tumor cells in the presence of CB307, leading to (**F**) PSMA-dependent secretion of IFNγ, (**G**) PSMA-dependent production of granzyme B, and (**H**) PSMA-dependent production of Bcl.xL. **I,** PSMA-dependent proliferation indicated by Ki67 expression. **J,** CB307 pharmacodynamic effects on NK cells. Statistical significance of CB307 treated versus untreated outcomes with PSMA-expressing tumor cells is indicated: **, $P < 0.01$; ****, $P < 0.0001$.

EC_{50} for CB307 induction of CD137 agonist reporter activity with DU145-PSMA cells was 0.120 (±0.24) nmol/L ($n = 3$). These data confirm the specificity of CB307 to agonize CD137 only in the presence of PSMA-expressing cells.

CB307-driven CD137 agonism induces T- and NK-cell activation

The PSMA-specific nature of CB307 to drive functional T-cell activities was also assessed using activated primary human immune cells (**Fig. 1E**). CB307 induced concentration-dependent increases in IFNγ production from PBMCs activated with anti-CD3 and cocultured with DU145-PSMA cells, but not when cocultured with DU145 parental cells (**Fig. 1F**). CB307 was able to elicit, in a PSMA-dependent manner, expected phenotypes in T cells resulting from CD137 agonism, including production of Granzyme B (**Fig. 1G**), induction of the anti-apoptotic protein Bcl-xL (**Fig. 1H**), and T-cell proliferation particularly in the $CD8^+$ compartment as shown by increased Ki67 expression (**Fig. 1I**).

CB307 also demonstrated activities consistent with the known activity of CD137 agonists on NK cells (28), again in a PSMA-dependent manner. Production of the chemokines CCL3 and CCL4, as well as IFNγ, each significantly increased when primary stimulated human NK cells were treated with CB307 in the presence of PSMA-expressing, but not PSMA-nonexpressing tumor cells (**Fig. 1J**). Together these data confirm that CB307 displays potent CD137 agonist activity only in the presence of PSMA-expressing cells.

CB307 combined with PD-(L)1 checkpoint inhibitors: (i) 2D cell cocultures

The functional activity of CB307 was tested in combination with antagonistic anti-PD-1 or anti-PD-L1 antibodies, to investigate the potential for synergy with established immunotherapies. PBMCs from healthy human donors were stimulated with SEB toxin, cocultured with DU145-PSMA cells and treated with CB307, anti-PD-1 antibody, anti-PD-L1 antibody or various combinations (**Fig. 2A**). IL2 was measured in coculture supernatants as a biomarker of T-cell activity.

When treated alone, CB307, the anti-PD-1 antibody, and the anti-PD-L1 antibody increased co-culture IL2 production by 2.01 (±0.28) fold, 1.61 (±0.23) fold, and 1.76 (±0.33) fold compared with untreated cells, respectively. The response was significantly increased upon combination treatment, with a mean (±SD) fold change in IL2 concentration of 2.9 (±0.20) with anti-PD-1 antibody ($P = 0.0002$),

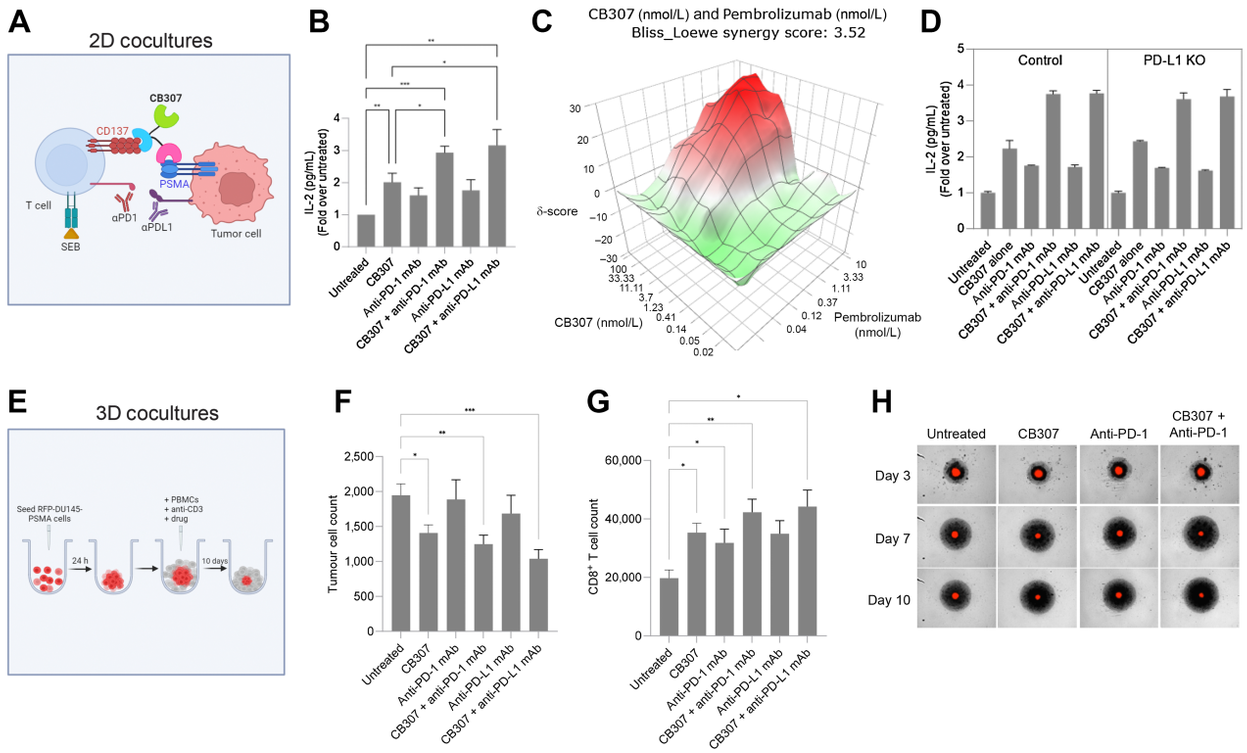

Figure 2.
CB307 activity in combination with immune checkpoint inhibitors. **A,** Schematic of a 2D primary cell-based experimental system assessing CB307 combination with immune checkpoint inhibitors. SEB is used to induce CD137 expression on primary T cells. **B,** IL2 secretion following drug treatment in the presence of PSMA-expressing tumor cells. Statistical significance: * $P < 0.05$, ** $P < 0.01$, *** $P < 0.001$. **C,** Isobologram of CB307-pembrolizumab additivity as assessed in 2D cocultures. **D,** Comparison of IL2 production between PD-L1–expressing versus PD-L1 CRISPR gene deleted nonexpressing tumor cells. In both cases, PSMA expression is similar. **E,** Schematic of a 3D tumor spheroid experimental system, whereby tumor cells fluoresce red whilst immune cells appear black. **F,** Single-agent versus combination drug activity measured as reduction in tumor cell count and (**G**) increasing $CD8^+$ T-cell count after 10 days in culture. Statistical significance: *, $P < 0.05$; **, $P < 0.01$; ***, $P < 0.001$. **H,** Changing red fluorescent tumor spheroid and surrounding black immune cell "cloud" over time.

and 3.16 (±0.49) with anti-PD-L1 antibody ($P = 0.0035$; $n = 5$; **Fig. 2B**).

To investigate the potential for synergy between CB307 and the anti-PD-1 antibody pembrolizumab, both molecules were titrated in the 2D *in vitro* coculture model with SEB-activated PBMCs, adopting a checkerboard design. IL2 production across this matrix was analyzed using SynergyFinder open source software (25), using a Bliss/Loewe consensus scoring method where the resulting synergy score of 3.52 suggests that although the drugs have additive activities, drug interaction does not appear to be highly synergistic *in vitro* (**Fig. 2C**; Supplementary Fig. S6).

Because the DU145-PSMA cell line also expresses high levels of PD-L1, to disentangle the mechanism by which the combination of CB307 with a checkpoint inhibitor increases immunologic activity, we used CRISPR technology to knockout (KO) PD-L1 from DU145-PSMA cells. Flow cytometric analysis confirmed loss of PD-L1 expression and retained PSMA expression (Supplementary Fig. S7). We obtained nearly identical results from the PD-L1–expressing DU145-PSMA cells as from the PD-L1 CRISPR KO version (**Fig. 2D**). These indicate that PD-L1 expression on tumor cells is not driving the response to checkpoint inhibitors in this experimental system, and that the combination benefit is likely derived from stimulation of CD137 and inhibition of PD-1 signaling on PBMCs themselves. Our results in this regard are consistent with previous observations of immune checkpoint inhibitor pharmacodynamics in a tumor-cell–independent system, where PD-L1 expression on $CD4^+$ T cells, monocytes, and dendritic cells may be mediating the PD-1 T-cell response (29).

CB307 combined with PD-(L)1 checkpoint inhibitors: (ii) 3D spheroid cocultures

CB307 treatment of PSMA-expressing 3D tumor spheroids cocultured with αCD3-stimulated primary human PBMCs (**Fig. 2E**) caused a statistically significant ($P = 0.0355$) reduction in tumor cell numbers versus stimulated primary human PBMCs in the absence of CB307 treatment (**Fig. 2F**). PD-1 or PD-L1 inhibitors without CB307 had only a modest tumor growth inhibition effect. Combining CB307 with either a PD-1 or PD-L1 inhibitor increased the tumor growth inhibition versus single-agent CB307 ($P = 0.003$ and $P = 0.0001$, respectively). We also observed a significant increase in the number of $CD8^+$ T cells upon treatment with CB307 ($P = 0.0161$), and further increases in $CD8^+$ T cells when CB307 was combined with either an anti-PD-1 or anti-PD-L1 antibody ($P = 0.0092$ and 0.0496, respectively; **Fig. 2G**). The reduction in tumor cells and increase in T cells can be visualized in this system by a decrease in the size of the red fluorescent tumor spheroid and an increase in size in the surrounding "black cloud" of proliferating T cells, respectively (**Fig. 2H**; Supplementary Fig. S8; Supplementary Video S1).

Collectively, the combination *in vitro* pharmacology data presented provides a mechanistic underpinning for the combination of CB307 with checkpoint inhibitor therapeutics in clinical development.

Clinical relevance of PSMA-dependent CD137 targeting in human cancers

Validation and optimization of CD137 staining on control tissues resulted in a staining pattern consistent with expectations for CD137 expression (**Fig. 3A**; Supplementary Fig. S1). A survey of multitumor TMAs showed that PSMA expression was largely restricted to prostate cancer samples (**Fig. 3B**). CD137 expression showed considerable variability across tumor types and was highest in lymphomas (both Hodgkin and non-Hodgkin lymphomas) and lowest in bladder, brain, and prostate tumors (**Fig. 3C**).

We considered that commercially available tumor samples such as TMAs are generally constructed from archival surgical resections of primary tumors with unknown provenance and may differ from metastatic tumors. Accordingly, we determined the degree of PSMA- or CD137-expressing cells in a set of samples collected from a single clinical site. Samples included primary human prostate tumors as well as prostate cancer metastases to bone marrow, lymph node, soft tissue, and liver. PSMA expression was higher in primary tumors and in metastases to bone marrow, lymph node, and soft tissues, compared with substantially reduced PSMA expression in liver metastases (**Fig. 3D**). Interestingly, in our dataset there were almost no $CD137^+$ cells in either tumor or stroma from primary prostate cancer lesions, consistent with the data from prostate cancer TMA samples. In contrast, there was significant $CD137^+$ cell presence in sites of metastatic prostate cancer with tumoral $CD137^+$ cell densities generally lower than intrastromal $CD137^+$ cell densities (**Fig. 3E** and **F**). As was the case with PSMA expression, CD137 densities were in aggregate higher in prostate cancer metastases to bone marrow, lymph node, and soft tissues compared with $CD137^+$ cell density in liver metastases, particularly in the tumor-surrounding stromal tissue. Pathologist (B.G.) examination of hematoxylin and eosin (H&E) stained slides from prostate cancer liver metastases showed 4/10 samples either exhibited or were suspicious for neuroendocrine differentiation; however, lower levels of PSMA and CD137 expression were also observed in the liver metastases that did not show obvious neuroendocrine features (Supplementary Fig. S9), potentially due to epigenetic modification of PSMA expression (30).

Mouse *in vivo* pharmacology: (i) pharmacokinetics

CB307 pharmacokinetics in mice and NHPs is shown in **Fig. 4**. The impact of species-specific serum albumin and FcRn-mediated drug recycling was demonstrated with plasma exposure in NCG mice that express neither human albumin nor the human FcRn (**Fig. 4A**, Group 4), where the half-life of CB307 precursor was on the order of

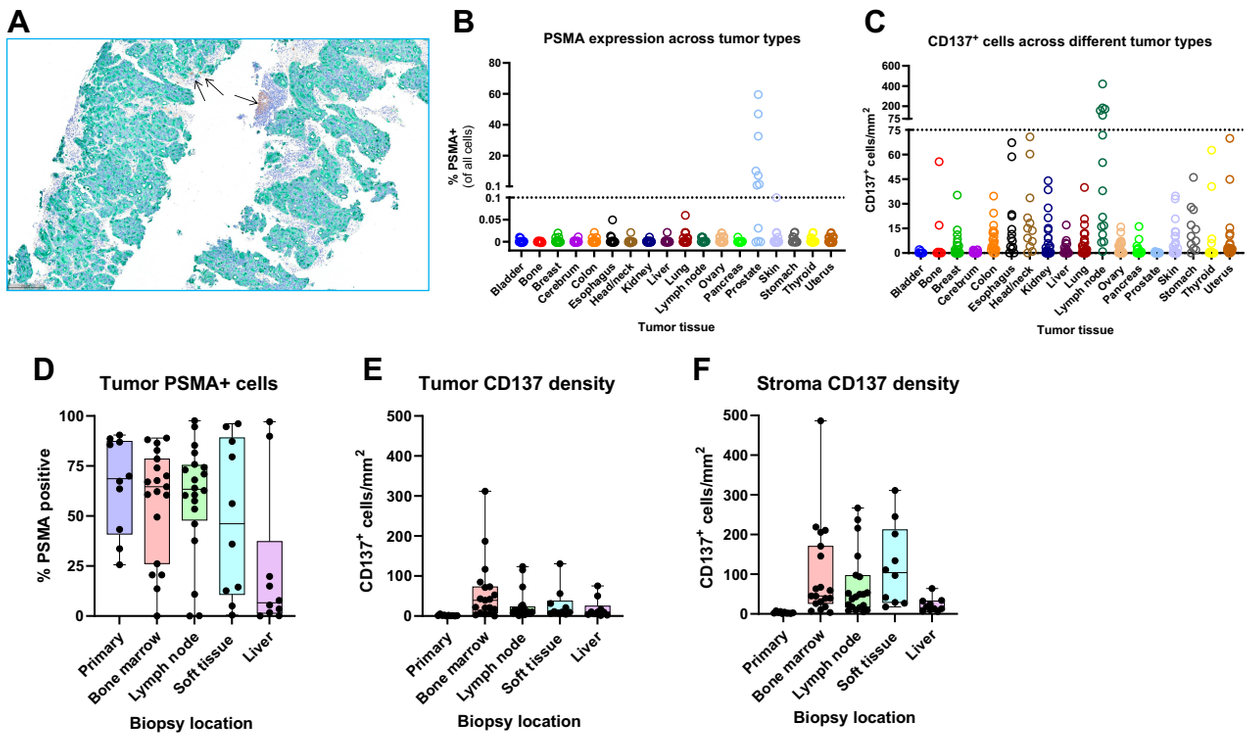

Figure 3.

PSMA and CD137 expression measured by IHC. **A,** Primary human prostate cancer tumor co-stained for PSMA (green) and CD137 (brown). Arrows indicate patches of CD137-positive cells. **B,** PSMA positivity across a selection of human multitumor tissue microarrays. Shown are percent of cells in a core showing any level of PSMA positivity by IHC as quantified by image analysis. Where duplicate cores have been stained and scored, results are presented as the average. **C,** Density of CD137-positive cells per mm^2 of viable tissue. Cells with any level of CD137 expression as determined by image analysis of IHC staining on sample cores are shown. Where duplicate cores have been stained and scored, results are presented as the average. **D,** PSMA expression in sites of primary and metastatic human prostate cancer are shown—any level of PSMA expression in a given cell is counted as positive. The median value for each anatomical site is indicated. Boxes represent inner quartiles. Each dot represents a sample from an individual patient. **E,** CD137-positive cell density in regions determined by image analysis to be tumor. **F,** The density of CD137-positive cells in the tumor-adjacent nontumor stromal tissue.

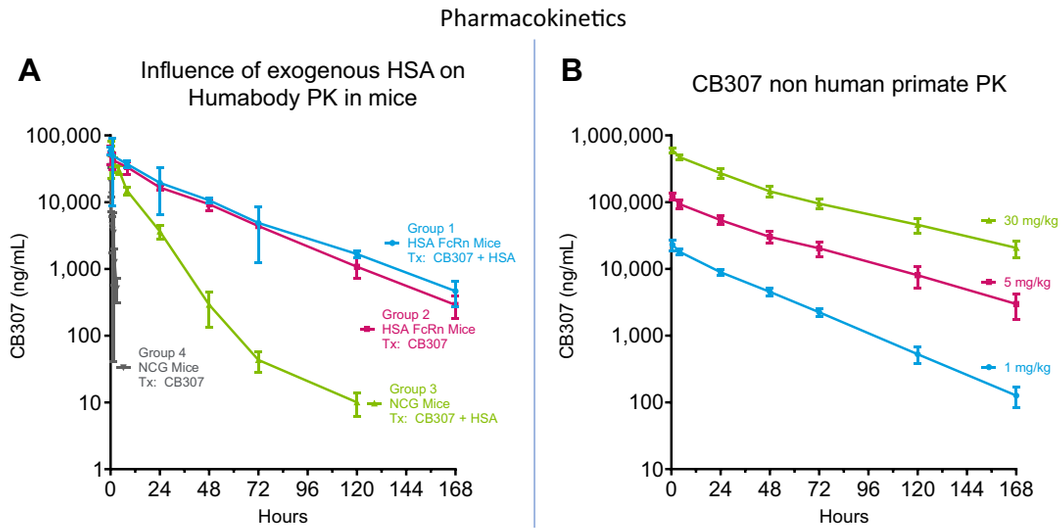

Figure 4.

Pharmacokinetic properties of CB307 and related molecules in mice and NHPs. **A,** A three-V_H precursor molecule to CB307 *in vivo* plasma concentration following single-dose injection into mice. CB307 precursor PK is shown with and without exogenous HSA addition, in mice either wild-type or humanized for albumin and FcRn ("NCG" and "HSA FcRn," respectively). **B,** CB307 plasma concentration over time following single-dose intravenous injection of three different dose levels in cynomolgus macaques. Error bars in **A** and **B** represent the SD of the individual measurements.

45 minutes, consistent with anticipated rapid renal clearance (31) of proteins with a molecular weight of 46 kDa. Pre-mixing CB307 precursor with exogenous HSA sufficed to significantly extend the drug's serum half-life to over 11 hours (**Fig. 4A**, Group 3). As expected, coadministration of exogenous HSA with the CB307 precursor molecule in mice transgenic for both HSA and hFcRn did not significantly impact the serum half-life of the CB307 precursor compared with CB307 precursor administration alone in the HSA/hFcRn model (**Fig. 4A**, Groups 1 and 2, respectively), in both cases with a half-life of slightly over 1 day. The half-life extension demonstrated in group 4 for drug co-dosed with HSA, albeit not as effective as that from HSA/hFcRn transgenic mice, was sufficient to enable implementation of mouse *in vivo* efficacy studies in mice transgenic for hCD137, but wild-type for both mouse albumin and FcRn, dosing CB307 itself rather than a murine albumin binding surrogate molecule. Full mouse summary PK statistics are shown in Supplementary Table S1.

Mouse *in vivo* pharmacology: (ii) antitumor activity

CB307 when coadministered with HSA was well-tolerated by RM-1-hPSMA tumor-bearing mice in the designed dosing regimens, illustrated in **Fig. 5A**. CB307 displayed increased antitumor activities from day 7 to day 24. All three dose levels of CB307 tested demonstrated approximately equivalent antitumor activity relative to the HSA-only dosed control group (**Fig. 5B**). In the HSA control group tumors grew in size until day 10, at which point most animals demonstrated a temporary and limited reduction in tumor size with tumor escaping growth control by day 21. This observation suggests an initial immunogenic response to induced expression of human PSMA in mice which is insufficient to clear the tumor. In contrast, mice treated with CB307 were able to consolidate this initial antitumor response, consistent with the T-cell costimulatory mechanism of CD137 agonism (32), resulting in deep tumor size regressions by day 24 of treatment relative to the peak of tumor growth around day 10, including in some cases regressions below the tumor volume at which treatment was initiated on study day 0. Almost all animals, including those in the CB307-treated groups, began to lose tumor growth control by day 28, perhaps because, notwithstanding the continuous exposure of the mice to doxycycline to induce hPSMA expression in the tumors, high tumor hPSMA expression on day 7 had decreased substantially by day 14 (Supplementary Fig. S10) suggesting hPSMA expression could not be constitutively sustained in this model system, even in the absence of selective pressure against hPSMA expression from CB307.

Interestingly, in this range of doses tested there was no obvious dose/response relationship and no evidence of a prozone or "hook effect" (33) reduction in antitumor activity at the highest 10 mg/kg CB307 dose level. The tumor volumes on day 24 in the three CB307-treated groups were not appreciably different from group to group (Kruskal–Wallis test for $k = 3$) and each CB307-treated group was individually statistically distinct with respect to the HSA-only treated control group (Mann–Whitney test; assessed using VassarStats (RRID: SCR_010263; **Fig. 5C**). The heterogeneity of response within a given group is a characteristic of syngeneic models generally (34).

CB307 NHP toxicology and toxicokinetics

In a GLP toxicology study in cynomolgus macaques, there were no unscheduled deaths, nor changes in body weight, ophthalmic examinations, electrocardiology, coagulation, clinical chemistry or urinalysis, or cytokine release considered related to CB307. There were no gross findings or organ weight changes associated with administration of CB307.

There were no adverse clinical observations in any animals following two doses of CB307 (on day 1 and 8). However, adverse clinical signs consistent with an acute hypersensitivity response were noted during the infusion in the first four males in the low dose group (1 mg/kg/dose), following CB307 administration on the third dosing occasion (day 15). Consequently, upon veterinary advice, the infusion of these animals was stopped (with these animals only receiving a partial dose ranging from 18% to 31% of the total intended dosing volume) and the other animals in this group and animals in higher dose groups (5 or 30 mg/kg/dose) were not administered a third dose.

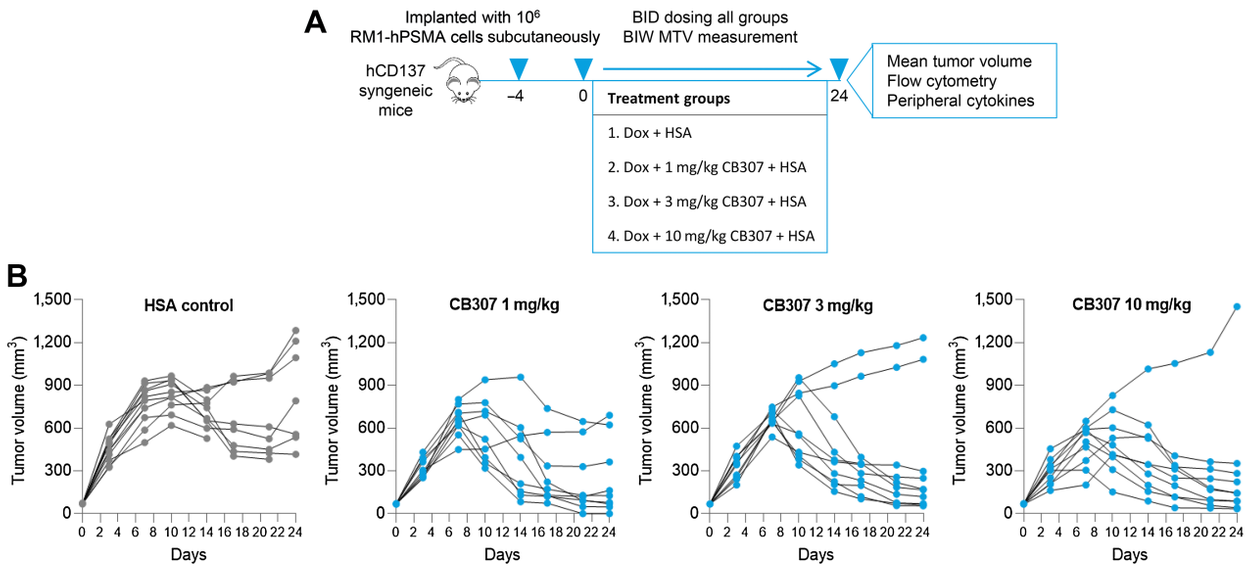

C

Day 24	HSA control	CB307 1 mg/kg	CB307 3 mg/kg	CB307 10 mg/kg
Mean tumor volume (mm^3)	841.93	240.42	351.48	285.38
SEM	133.97	86.09	137.30	133.81
Group size	7	9	10	10
Kruskal–Wallis CB307 groups		$P = 0.82$		
Mann–Whitney vs. control		$P = 0.008$	$P = 0.017$	$P = 0.007$

Figure 5.

In vivo pharmacology of CB307 in syngeneic mouse tumor models. **A,** *In vivo* pharmacology study scheme. **B,** Individual animal tumor size graphs over time. HSA control (gray symbols) contrasts with CB307 co-injected with HSA (blue symbols). Indicated drugs were administered twice per day. **C,** Statistics of end-of-study tumor volumes.

Clinical parameters of individual animals displaying an immune-mediated hypersensitivity response had generally returned to pre-treatment levels by 24 hours after dosing. Increases in the liver enzyme aspartate aminotransferase and increased C-reactive protein noted 24 hours after dose in three of the four animals were possibly related to an acute inflammatory response associated with immune complex clearance in the liver as a secondary effect of ADA formation (35). All parameters normalized within 72 hours (the next scheduled time point) of the third 1 mg/kg dose and no liver histopathologic findings were noted. Similar immunogenic findings with human biological entities dosed to nonhuman species in nonclinical studies have been observed previously and are not considered predictive of immunogenicity responses in the clinic (36).

Following a single 30-minute intravenous infusion administration, the increase in systemic exposure to CB307 on day 1 (based on C_{max} and AUC_{inf} values) was linear and dose-proportional from 1 to 30 mg/kg/dose. Half-life ($t_{1/2}$) was slightly longer as dose increased from 1 to 30 mg/kg/dose for males and females on day 1 (**Fig. 4B**). No sex-related differences in systemic exposure to CB307 were noted across the dose range. TK summary statistics from a single administered dose are shown in **Table 1**. Allometric scaling predicts that the CB307–albumin complex will have a mean terminal half-life in human patients of 3.5 days.

Discussion

CB307 potently binds to PSMA- and CD137-expressing cells and enhances T- and NK-cell function through CD137 agonism. Intentionally, the CB307 requirement for colocalization of cell presented PSMA with CD137-expressing cells to effect CD137 agonism restricts CB307 enhancement of immune cell activity to regions, such as the tumor microenvironment of prostate cancer metastatic lesions, in which both targets are present. By this means, we hope to avoid the toxicities found with first-generation CD137 agonists resulting from CD137 expression broadly on immune cells in the periphery, liver, and other on-target off-tumor organs (37). Although CB307 is, to our knowledge, the first-in-class clinical asset for using PSMA expression to restrict drug-mediated CD137 agonism, this type of tumor-antigen conditional CD137 agonism is a contemporary therapeutic approach with encouraging data reported by targeting CD137 agonism to other tumor-associated antigens including HER2 (38), FAP (39), and PD-L1 (40, 41).

Multispecific molecules when applied *in vitro* at high concentrations can exhibit a prozone or "hook effect," whereby monospecific saturation of the individual targets replaces intramolecular bridging between the targets leading to a reduction in functional activity (42). As expected, we can observe such an effect *in vitro* with CB307; we do not,

Table 1. Sex-combined summarized toxicokinetic parameters of CB307 in cynomolgus macaque serum following 30-minute intravenous infusion administration of CB307 at 1, 5, and 30 mg/kg/dose on day 1.

Dose (mg/kg per dose)	Statistical analysis	C_{max} (μg/mL)	C_{max} /dose (μg/mL)/ (mg/kg/dose)	AUC_{tlast} (μg·day/mL)	AUC_{tlast}/dose (μg·day/mL)/ (mg/kg/dose)	AUC_{inf} (μg·day/mL)	$t_{1/2}$ (*h*)
1	Mean	23.5	23.5	28.4	28.4	28.6	22.5
	SD	3.38	3.38	2.55	2.55	2.60	2.02
5	Mean	122	24.4	187	37.4	193	34.2
	SD	14.6	2.92	33.5	6.70	36.6	3.17
30	Mean	603	20.1	941	31.4	995	42.7
	SD	54.4	1.81	130	4.34	148	3.78

Note: All time-related parameters have been calculated from the start of the 30-minute intravenous infusion administration.
Abbreviations: AUC_{inf}, area under the curve from time of dosing extrapolated to time=infinity; AUC_{tlast}, area under the curve at the time of last measurable concentration.

however, see any evidence of drug oversaturation leading to reduction of antitumor activity *in vivo* over a 10-fold range of drug dose levels in syngeneic mouse tumor models. Notably, the plasma half-life of CB307 in both transgenic mice and cynomolgus macaques is considerably shorter than the half-life of traditional mAb, whereby we hypothesize that the relatively flat dose/response relationship of CB307 and the lack of a hook effect arises from transient sampling of optimal drug concentration for CD137 agonism over the dosing interval. Indeed, as sustained T-cell signaling may promote an exhausted T-cell phenotype (43), it may well prove advantageous for an agonist therapeutic to have a shorter plasma half-life than checkpoint inhibitors which require sustained target coverage.

The pharmacokinetic characteristics of CB307 enable weekly clinical administration for sustained target coverage, where allometric modeling from nonclinical data predicts an approximate four-fold range of exposure over the dosing interval, or potentially biweekly administration for a more pulsatile exposure approach. In our hands, V_H-based molecules have pharmacokinetic properties that seem to be significantly determined by choice of V_H employed for HSA binding where selection of alternative HSA-binding V_H permits a degree of pharmacokinetics "tuning." In addition, there are several well-established possibilities for half-life extension other than through HSA-binding V_H moieties (44), including direct fusions to albumin itself, PEGylation, and/or fusion to an appropriate antibody-based Fc-domain.

Although prostate cancer has been considered to be an "immunologically cold" tumor type (45), our data assessing the co-prevalence of CD137-expressing cells with PSMA-expressing tumor cells in various metastatic tumor lesion settings support a role for CD137 therapeutics in the treatment of metastatic prostate cancer. More broadly, whilst results of checkpoint inhibitors in prostate cancer have been disappointing (46), a combination approach may be a way forward for checkpoint inhibitors (47) in this historically difficult tumor type. Accordingly, our preclinical data showing the increased activity of a conditional CD137 agonist when combined with PD-(L)1 checkpoint inhibitors, independent of PD-L1 expression on tumor cells, support clinical exploration of such a combination.

Emerging characterization of the capacity for the mCRPC approved radiotherapeutic ^{177}Lutetium-PSMA-617 (^{177}Lu vipivotide tetraxetan) to induce immunogenic cell death (48) suggests another potential path for clinical development in combination with CB307. To be tested is that nascent antitumor immunologic responses triggered by ^{177}Lu-mediated cellular damage could be consolidated through localized CD137 costimulation. Addressing the feasibility of this hypothesis, we have determined that although vipivotide tetraxetan and CB307 both target PSMA, even relatively high levels of vipivotide tetraxetan do not appreciably inhibit the PSMA-dependent function of CB307 (Supplementary Fig. S11). Early reporting of clinical findings resulting from combining ^{177}Lu vipivotide tetraxetan with the checkpoint inhibitor pembrolizumab have also been promising (49), such that in the future, as the standard of care in mCRPC continues to evolve, immunoradiotherapy combined with immunotherapy such as CB307 could be considered.

Notably, although the T-cell–enhancing CD137 agonism activity of CB307 is localized to and contingent upon microenvironmental regions of PSMA positivity, the polyclonally stimulated T cells retain specificity against their cognate tumor antigens, which may or may not include PSMA itself. Because heterogeneity in PSMA expression is common in CRPC (44, 45), CB307's ability to stimulate polyclonal T-cell–mediated antitumor responses, including against PSMA-negative cells, could overcome resistance mechanisms that may impact PSMA-directed bispecific T-cell engager (BiTE) therapeutics (50, 51), which, by ligating T cells directly to PSMA-expressing tumors, may prove to be comparatively dependent upon homogeneous tumor PSMA expression for activity. In the future, combinations of CD3-engagers with tumor antigen–mediated T-cell enhancers such as CB307 may provide an additional route for clinical development.

In summary, CB307 is a potent and PSMA-dependent T-cell–enhancing half-life extended bispecific Humabody with promising therapeutic potential in PSMA-positive tumors. Clinical studies exploring use of monotherapy CB307 and the PD-1 inhibitor pembrolizumab combined with CB307 for the treatment of solid tumors (NCT04839991) and a radiolabeled-CB307 drug biodistribution study (NCT05836623) are currently open for patient accrual.

Authors' Disclosures

C. Guo reports employment with Genentech Inc. V. Brucklacher-Waldert reports other support from Revvity outside the submitted work. M. Maginn reports personal fees from Crescendo Biologics Ltd. during the conduct of the study and outside the submitted work. J. Legg reports other support from AstraZeneca and Mestag Therapeutics outside the submitted work and has a patent for WO2020229844A1 pending and a patent for CN111683968A pending. J.S. de Bono reports grants and personal fees from Crescendo Biologics Ltd. during the conduct of the study as well as grants and personal fees from Amgen, AstraZeneca, Astellas, Bayer, CellCentric, Daiichi, Genentech/Roche, Harpoon, Janssen, Merck Serono, Merck Sharp & Dohme, MetaCurUm, Myricx, Nurix Therapeutics, Oncternal, Orion Pharma, Pfizer, Sanofi Aventis, Sierra Oncology, and Taiho; personal fees from BioXcel Therapeutics, Boehringer Ingelheim, Dark Blue Therapeutics, Eisai, Genmab, GSK, ImCheck Therapeutics, Menarini/Silicon Biosystems, Novartis, Qiagen, Takeda, Tango Therapeutics, Terumo, and Vertex Pharmaceuticals; and grants from Immunic Therapeutics outside the submitted work. A.J. Pierce reports a patent for WO2019092452 pending to Crescendo Biologics Ltd. No disclosures were reported by the other authors.

Authors' Contributions

S. Archer: Conceptualization, data curation, formal analysis, supervision, investigation, methodology, writing–original draft, writing-review and editing. **P.M. Brailey:** Investigation, methodology, writing–original draft. **M. Song:** Investigation, methodology, writing–original draft. **P.D. Bartlett:** Investigation, methodology, writing–original draft. **I. Figueiredo:** Investigation, visualization, methodology, writing–original draft. **B. Gurel:** Investigation, visualization, methodology. **C. Guo:** Investigation, visualization, methodology, writing–review and editing. **V. Brucklacher-Waldert:** Investigation, methodology. **H.L. Thompson:** Investigation, methodology. **J. Akinwale:** Data curation, investigation, methodology. **S.E. Boyle:** Conceptualization, investigation. **C. Rossant:** Investigation, methodology. **N.R. Birkett:** Investigation, methodology. **J. Pizzey:** Investigation, methodology. **M. Maginn:** Formal analysis, supervision, methodology. **J. Legg:** Investigation, methodology. **R. Williams:** Resources, investigation, methodology. **C.M. Johnston:** Resources, investigation, methodology. **P. Bland-Ward:** Conceptualization, supervision, writing–review and editing. **J.S. de Bono:** Conceptualization, resources, supervision, methodology. **A.J. Pierce:** Conceptualization, formal analysis, supervision, funding acquisition, visualization, writing–original draft, writing–review and editing.

Acknowledgments

The authors thank the Crescendo CB307 project team, technical staff, and colleagues past and present for their support. All work was funded by Crescendo Biologics Ltd.

Note

Supplementary data for this article are available at Clinical Cancer Research Online (http://clincancerres.aacrjournals.org/).

Received October 6, 2023; revised December 7, 2023; accepted February 5, 2024; published first April 9, 2024.

References

1. von Amsberg G, Alsdorf W, Karagiannis P, Coym A, Kaune M, Werner S, et al. Immunotherapy in advanced prostate cancer—light at the end of the tunnel? Int J Mol Sci 2022;23:2569.
2. Sheehan B, Guo C, Neeb A, Paschalis A, Sandhu S, de Bono JS. Prostate-specific membrane antigen biology in lethal prostate cancer and its therapeutic implications. European Urology Focus 2022;8:1157–68.
3. Chang SS, O'Keefe DS, Bacich DJ, Reuter VE, Heston WD, Gaudin PB. Prostate-specific membrane antigen is produced in tumor-associated neovasculature. Clin Cancer Res 1999;5:2674–81.
4. Schmidt LH, Heitkötter B, Schulze AB, Schliemann C, Steinestel K, Trautmann M, et al. Prostate specific membrane antigen (PSMA) expression in non-small cell lung cancer. PLoS One 2017;12:e0186280.
5. Salas Fragomeni RA, Amir T, Sheikhbahaei S, Harvey SC, Javadi MS, Solnes LB, et al. Imaging of nonprostate cancers using PSMA-targeted radiotracers: rationale, current state of the field, and a call to arms. J Nucl Med 2018;59:871–7.
6. Nomura N, Pastorino S, Jiang P, Lambert G, Crawford JR, Gymnopoulos M, et al. Prostate specific membrane antigen (PSMA) expression in primary gliomas and breast cancer brain metastases. Cancer Cell Int 2014;14:26.
7. Bouchelouche K, Choyke PL, Capala J. Prostate specific membrane antigen-a target for imaging and therapy with radionuclides. Discov Med 2010;9:55–61.
8. Hofman MS, Lawrentschuk N, Francis RJ, Tang C, Vela I, Thomas P, et al. Prostate-specific membrane antigen PET-CT in patients with high-risk prostate cancer before curative-intent surgery or radiotherapy (proPSMA): a prospective, randomised, multicentre study. Lancet 2020;395:1208–16.
9. Houshmand S, Lawhn-Heath C, Behr S. PSMA PET imaging in the diagnosis and management of prostate cancer. Abdom Radiol (NY) 2023;48:3610–23.
10. Sartor O, de Bono J, Chi KN, Fizazi K, Herrmann K, Rahbar K, et al. Lutetium-177–PSMA-617 for metastatic castration-resistant prostate cancer. N Engl J Med 2021;385:1091–103.
11. Shuford WW, Klussman K, Tritchler DD, Loo DT, Chalupny J, Siadak AW, et al. 4–1BB costimulatory signals preferentially induce CD8+ T cell proliferation and lead to the amplification *in vivo* of cytotoxic T cell responses. J Exp Med 1997;186:47–55.
12. Hashimoto K. CD137 as an attractive T cell co-stimulatory target in the TNFRSF for immuno-oncology drug development. Cancers (Basel) 2021;13:2288.
13. Teijeira A, Labiano S, Garasa S, Etxeberria I, Santamaría E, Rouzaut A, et al. Mitochondrial morphological and functional reprogramming following CD137 (4–1BB) costimulation. Cancer Immunol Res 2018;6:798–811.
14. Menk AV, Scharping NE, Rivadeneira DB, Calderon MJ, Watson MJ, Dunstane D, et al. 4–1BB costimulation induces T cell mitochondrial function and biogenesis enabling cancer immunotherapeutic responses. J Exp Med 2018;215:1091–100.
15. Vinay DS, Kwon BS. Immunotherapy of cancer with 4–1BB. Mol Cancer Ther 2012;11:1062–70.
16. Lee HW, Park SJ, Choi BK, Kim HH, Nam KO, Kwon BS. 4–1BB promotes the survival of CD8+ T lymphocytes by increasing expression of Bcl-xL and Bfl-1. J Immunol 2002;169:4882–8.
17. Gilbreth RN, Oganesyan VY, Amdouni H, Novarra S, Grinberg L, Barnes A, et al. Crystal structure of the human 4–1BB/4–1BBL complex. J Biol Chem 2018;293:9880–91.
18. Chin SM, Kimberlin CR, Roe-Zurz Z, Zhang P, Xu A, Liao-Chan S, et al. Structure of the 4–1BB/4–1BBL complex and distinct binding and functional properties of utomilumab and urelumab. Nat Commun 2018;9:4679.
19. Yu X, James S, Felce JH, Kellermayer B, Johnston DA, Chan HTC, et al. TNF receptor agonists induce distinct receptor clusters to mediate differential agonistic activity. Commun Biol 2021;4:772.
20. Segal NH, Logan TF, Hodi FS, McDermott D, Melero I, Hamid O, et al. Results from an integrated safety analysis of urelumab, an agonist anti-CD137 monoclonal antibody. Clin Cancer Res 2017;23:1929–36.
21. Segal NH, He AR, Doi T, Levy R, Bhatia S, Pishvaian MJ, et al. Phase I study of single-agent utomilumab (PF-05082566), a 4–1BB/CD137 agonist, in patients with advanced cancer. Clin Cancer Res 2018;24:1816–23.
22. Teng Y, Young JL, Edwards B, Hayes P, Thompson L, Johnston C, et al. Diverse human VH antibody fragments with bio-therapeutic properties from the crescendo mouse. N Biotechnol 2020;55:65–76.
23. Nessler I, Khera E, Vance S, Kopp A, Qiu Q, Keating TA, et al. Increased tumor penetration of single-domain antibody-drug conjugates improves *in vivo* efficacy in prostate cancer models. Cancer Res 2020;80:1268–78.
24. Dennis MS, Zhang M, Meng YG, Kadkhodayan M, Kirchhofer D, Combs D, et al. Albumin binding as a general strategy for improving the pharmacokinetics of proteins. J Biol Chem 2002;277:35035–43.
25. Ianevski A, Giri AK, Aittokallio T. SynergyFinder 3.0: an interactive analysis and consensus interpretation of multi-drug synergies across multiple samples. Nucleic Acids Res 2022;50:W739–43.
26. Bausch-Fluck D, Hofmann A, Bock T, Frei AP, Cerciello F, Jacobs A, et al. A mass spectrometric-derived cell surface protein atlas. PLoS One 2015;10:e0121314.
27. Viuff D, Antunes F, Evans L, Cameron J, Dyrnesli H, Thue Ravn B, et al. Generation of a double transgenic humanized neonatal Fc receptor (FcRn)/albumin mouse to study the pharmacokinetics of albumin-linked drugs. J Control Release 2016;223:22–30.
28. Cabo M, Santana-Hernández S, Costa-Garcia M, Rea A, Lozano-Rodríguez R, Ataya M, et al. CD137 costimulation counteracts TGFβ inhibition of NK-cell antitumor function. Cancer Immunol Res 2021;9:1476–90.
29. Mellman I, Chen DS, Powles T, Turley SJ. The cancer-immunity cycle: Indication, genotype, and immunotype. Immunity 2023;56:2188–205.
30. Sayar E, Patel RA, Coleman IM, Roudier MP, Zhang A, Mustafi P, et al. Reversible epigenetic alterations mediate PSMA expression heterogeneity in advanced metastatic prostate cancer. JCI Insight 2023;8:e162907.
31. Li Z, Krippendorff BF, Shah DK. Influence of molecular size on the clearance of antibody fragments. Pharm Res 2017;34:2131–41.
32. Chester C, Sanmamed MF, Wang J, Melero I. Immunotherapy targeting 4–1BB: mechanistic rationale, clinical results, and future strategies. Blood 2018;131:49–57.
33. Bray D, Lay S. Computer-based analysis of the binding steps in protein complex formation. Proc Natl Acad Sci USA 1997;94:13493–8.

34. Yu JW, Bhattacharya S, Yanamandra N, Kilian D, Shi H, Yadavilli S, et al. Tumor-immune profiling of murine syngeneic tumor models as a framework to guide mechanistic studies and predict therapy response in distinct tumor microenvironments. PLoS One 2018;13:e0206223.
35. Krishna M, Nadler SG. Immunogenicity to biotherapeutics—the role of anti-drug immune complexes. Front Immunol 2016;7:21.
36. Husar E, Solonets M, Kuhlmann O, Schick E, Piper-Lepoutre H, Singer T, et al. Hypersensitivity reactions to obinutuzumab in cynomolgus monkeys and relevance to humans. Toxicol Pathol 2017;45:676–86.
37. Bartkowiak T, Jaiswal AR, Ager CR, Chin R, Chen CH, Budhani P, et al. Activation of 4–1BB on liver myeloid cells triggers hepatitis via an interleukin-27-dependent pathway. Clin Cancer Res 2018;24:1138–51.
38. Hinner MJ, Aiba RSB, Jaquin TJ, Berger S, Dürr MC, Schlosser C, et al. Tumor-localized costimulatory T-cell engagement by the 4–1BB/HER2 bispecific antibody-anticalin fusion PRS-343. Clin Cancer Res 2019;25:5878–89.
39. Melero I, Tanos T, Bustamante M, Sanmamed MF, Calvo E, Moreno I, et al. A first-in-human study of the fibroblast activation protein–targeted, 4–1BB agonist RO7122290 in patients with advanced solid tumors. Sci Transl Med 2023;15:eabp9229.
40. Peper-Gabriel JK, Pavlidou M, Pattarini L, Morales-Kastresana A, Jaquin TJ, Gallou C, et al. The PD-L1/4–1BB bispecific antibody-anticalin fusion protein PRS-344/S095012 elicits strong T-cell stimulation in a tumor-localized manner. Clin Cancer Res 2022;28:3387–99.
41. Muik A, Garralda E, Altintas I, Gieseke F, Geva R, Ben-Ami E, et al. Preclinical characterization and Phase I trial results of a bispecific antibody targeting PD-L1 and 4–1BB (GEN1046) in patients with advanced refractory solid tumors. Cancer Discov 2022;12:1248–65.
42. Jacobs JFM, van der Molen RG, Bossuyt X, Damoiseaux J. Antigen excess in modern immunoassays: to anticipate on the unexpected. Autoimmun Rev 2015;14:160–7.
43. Miggelbrink AM, Jackson JD, Lorrey SJ, Srinivasan ES, Waibl-Polania J, Wilkinson DS, et al. CD4 T-cell exhaustion: does it exist and what are its roles in cancer? Clin Cancer Res 2021;27:5742–52.
44. Ogihara T, Mizoi K, Ishii-Watabe A. Pharmacokinetics of biopharmaceuticals: their critical role in molecular design. Biomedicines 2023;11:1456.
45. Stultz J, Fong L. How to turn up the heat on the cold immune microenvironment of metastatic prostate cancer. Prostate Cancer Prostatic Dis 2021;24:697–717.
46. Merck.com [Internet]. [cited 2023 Aug 3]. Merck Provides Update on Phase 3 Trials KEYNOTE-641 and KEYNOTE-789. Available from: https://www.merck.com/news/merck-provides-update-on-phase-3-trials-keynote-641-and-keynote-789/
47. Plas S, Pircher A, Heidegger I. Pembrolizumab in mCRPC—combination therapies as breakthrough to success? Curr Opin Urol 2023;33:458–71.
48. Ertveldt T, De Beck L, De Ridder K, Locy H, de Mey W, Goyvaerts C, et al. Targeted radionuclide therapy with low and high-dose Lutetium-177-labeled single domain antibodies induces distinct immune signatures in a mouse melanoma model. Mol Cancer Ther 2022;21:1136–48.
49. Sandhu S, Joshua AM, Emmett L, Spain LA, Horvath L, Crumbaker M, et al. PRINCE: Phase I trial of 177Lu-PSMA-617 in combination with pembrolizumab in patients with metastatic castration-resistant prostate cancer (mCRPC). JCO 2022;40(16_suppl):5017.
50. Deegen P, Thomas O, Nolan-Stevaux O, Li S, Wahl J, Bogner P, et al. The PSMA-targeting half-life extended BiTE therapy AMG 160 has potent antitumor activity in preclinical models of metastatic castration-resistant prostate cancer. Clin Cancer Res 2021;27:2928–37.
51. Hummel HD, Kufer P, Grüllich C, Seggewiss-Bernhardt R, Deschler-Baier B, Chatterjee M, et al. Pasotuxizumab, a BiTE® immune therapy for castration-resistant prostate cancer: Phase I, dose-escalation study findings. Immunotherapy 2021;13:125–41.